EXPERIMENTAL INVESTIGATION OF COLD-SPRAY CHROMIUM CLADDING

M. SHAHIN[a], J. PETRIK[a,b],
[a] *Department of Nuclear Science and Engineering, Massachusetts Institute of Technology*
77 Massachusetts Ave, Cambridge, MA, 02139, USA

A. SESHADRI[a], B. PHILLIPS[a], K. SHIRVAN[a]
[b] *Faculty of Mechanical Engineering, Czech Technical University in Prague*
Technicka 4, Praha 6, 166 07, Czech Republic

ABSTRACT

This paper investigates the experimental performance of cold-spray chromium (Cr) coating on Zircaloy-4. Previously, preliminary steam and autoclave testing along with thermo-mechanical modelling showed Cr-coating via cold spray process is a promising accident tolerant fuel (ATF) concept. In this work, optimized Cr coating under high-temperature steam (1200 °C), rod burst and high-temperature quench are investigated. The result indicates that Cr coating provides adequate protection against oxidation and reduces hydrogen pickup and generation. Though a failure mode in terms of assembly buckling could be realized at < 1300 °C. The in-reactor thermal hydraulic performance of the Cr coating should also be similar to Zircaloy based on detailed surface characterization and quench performance.

1 Introduction

Accident Tolerant Fuels (ATF) are defined as nuclear fuels that can tolerate severe accident conditions in a Light Water Reactor (LWR) for a considerably longer time compared to reference fuel system while maintaining or improving fuel performance in nominal operating conditions, Anticipated Operational Occurrences (AOOs) and postulated accidents [1]. The chromium (Cr) coated cladding is a near-term ATF option pursued by various groups. Chromium plating has also been widely used to improve the corrosion resistance of structures. Currently, both AREVA [2] and Westinghouse [3] are pursuing Cr-coated cladding to be inserted in commercial reactors in the US as part of the Department of Energy (DOE) ATF program.

The coatings can be deposited by various techniques such as chemical vapor deposition, physical vapor deposition, laser deposition, thermal spray, atomic layer deposition etc. [2] [3] [4] [5] [6]. In our work, cold-spray (CS) was used as the deposition technique. The previous work has shown preliminary steam and autoclave testing along with thermo-mechanical modelling of the cold spray Cr-coating, showing promising results [7]. In this work, optimized Cr coating under high-temperature steam (1200 °C), rod burst and high-temperature quench are investigated.

2 Materials and experimental setup

2.1 Materials

Standard commercially available Zircaloy-4 was used as a substrate for all tests. The composition is as follows: 1.32-Sn; 0.21-Fe; 0.11-Cr; 0.13-O; Bal-Zr. The substrate was surface polished in ethanol lubricant with 320 grit SiC abrasive paper before deposition of coatings. Pure Cr (deposited by Plasma Processes, LLC) was applied on the outer surface of the Zircaloy-4 tubes via a CS process. Uncoated and Cr-coated Zircaloy-4 pressure tubes are

shown as an example in Fig. 1. Uncoated Zircaloy-4 was also studied as the reference case after cleaning in DI water, ethanol and acetone in agreement with [8].

Fig. 1: Uncoated Zircaloy-4 sample (top) and Cr coated (bottom).

CS process involves the acceleration of micron-sized particles in the form of powders that are carried in a high pressure and sometimes heated gas stream (RT – 1200°C) in the solid state toward a suitable substrate. During the interaction with the substrate, the particle undergoes tremendous plastic deformation. Upon impact, the plastic deformation disrupts and breaks down surface oxide layers on both the powder and substrate leading to a metallurgical bond, as well as mechanical interlocking.

Comment [BP1]: What is RT?

In this study, using similar CS parameters as the previous study, the particle size of Cr was down-selected to 20 µm, thus producing a coating of 20 to 30 µm by Plasma Processes, LLC vs. 15 to 75 µm coating thickness in the previous work by a different manufacturer. In addition, for the pressure tube geometry shown in Fig. 1, a robotic arm was used to coat the entire sample at once. In the previous study, the coating was done on the cylindrical body. Then the sample was reoriented and the coating was then applied on the end-cap. This way, the presence of coating defects in the end cap weld region is minimized.

2.2 Experimental Setup

2.2.1 High-temperature steam oxidation experiment

High-temperature steam oxidation (HTSO) facility was built in 2015 at MIT to perform high-temperature steam oxidation experiments on cladding materials [9] [10]. The facility consists of a boiling pool, a quartz tube inside which steam passes and three stage heaters that heat the steam from outside of the quartz tube. The steam flow rate is driven by the 1800 W immersed heater whose input power is controlled through a DC power supply, thereby allowing accurate control of the steam flow rate. The desired steam flow rate is calibrated gravimetrically before each test. Testing is performed by suspending the sample in the furnace as the steam passes across. The last furnace temperature is measured by an OMEGA B-type thermocouple on the outside of the quartz tube with accuracy 3.0 ^{o}C at 1200 ^{o}C. Since there is no thermocouple inside the quartz tube in the last furnace, the oxidation temperature is calibrated by oxidizing multiple Zircaloy-4 samples since Zircaloy-4 follows Cathcart-Pawel correlation [11] used by Nuclear Regulatory Commission (NRC) at high temperatures. Uncertainty in the parabolic rate constant of Cathcart-Pawel correlation is reported to be 2.5% by the authors [11]. These

uncertainties along with the uncertainty in weight gain measurements of Zircaloy-4 sample propagate to a total uncertainty of 4.2 °C. HTSO facility can have oxidation temperature up to 1500 °C and maximum steam flow rate of 15 g/min. The design of the HTSO facility exposes the samples to very rapid temperature ramp rate. Basic heat balance estimates that the samples reach oxidation temperature in less than one second.

2.2.2 Quench experiment

Fig. 2 shows the experimental setup for the quench tests. Tested samples are cylindrical rodlets made of Zircaloy-4 (Sample 1) and Cr spray coated on Zircaloy-4 (Sample 2). The test sample is a cylindrical rodlet (test sample) of diameter 4.8 mm and height of 50 mm. The radiant furnace powered with a DC power supply (25 V, 150 A) is used to achieve a maximum temperature of 1500 °C. Pneumatic pressure (600 kPa) is used to displace the sample downward to the quench pool at a mean velocity of 0.5 m/s. The downward motion of the sample is actuated by a 4-way solenoid valve. The water in the quench pool is at saturation temperature (1 atm, 100 °C) and the temperature is controlled with the help of a hot plate and temperature controller. A K-type sheathed thermocouple is mounted on the top side of the test sample which is drilled to insert the sample and is connected to HP Agilent 34980A data acquisition system for online measurement of temperature. The temperature data is recorded at a rate of 20 Hz. The uncertainty in the measurement of temperature using the thermocouple is 2.2 °C. The visualization of the transient boiling during the quenching of surfaces is done using a high-speed CMOS camera (Vision Research Phantom V12.1). The high-speed camera was operated at 4800 fps at the 800 x 600-pixel resolution.

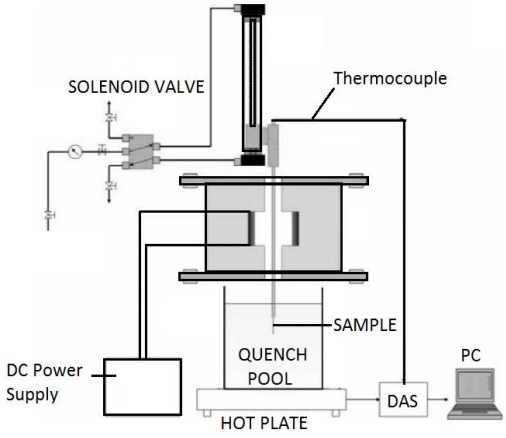

Fig. 2: Quench experimental setup

Contact angle and capillary wicking measurements were carried out by impinging three different droplets (20 µL) on the "as machined/received" samples. The average of three measurements at different locations was taken. Contact angle measurements were performed using a contact angle goniometer. The measurement of the contact angle and the capillary wicking is explained in Rahman *et al* [12]. The experimental uncertainty in the measurement of the wicking velocity is estimated as 0.1 mm^3/s. Initial quench and contact angle measurements were taken prior to

irradiation to serve as a reference to understand the effect of irradiation. A Gamma-cell 220E irradiator available at the MIT Biology department was used. The Gamma-cell 220E Irradiator uses 12 cobalt-60 pencil sources, arranged axially in a sample chamber. The integrated irradiation dose on the samples was in the range of 300-500 kGy.

2.2.3 Burst test

The burst test was performed with the help of test facility outlined in Fig. 3. Samples were sealed using plugs with O-rings and filled with hydraulic oil. The steel structure holding the sample is placed in an acrylic box that protects surroundings against a subsequent splash of the oil. Internal pressure is provided by the hand pump connected to the sample with piping and actual pressure is displayed on the analog gauge. Moreover, the whole process of sample pressurizing is recorded via a digital camera.

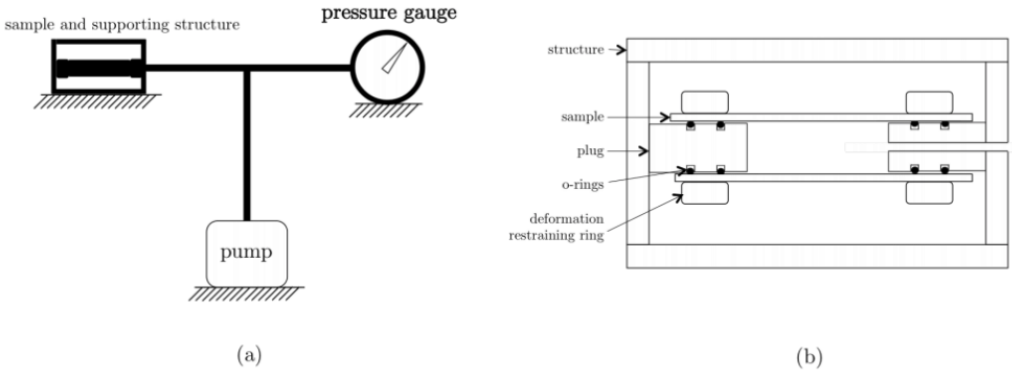

Fig. 3: Burst experimental setup. (a) test facility (b) sample with supporting structure.

3 Results

3.1 High Temperature Steam Oxidation

The Cr-coated Zircaloy-4 tube was inserted in the steam oxidation column. Steam oxidation tests was carried out at 1200°C with a steam mass flow rate of ~5.5 g/min. The sample was oxidized in three consequent stages for 15 minutes, 30 minutes, and 60 minutes with air quenching for 2 minutes after each stage. In contrast to previous high-temperature stem oxidation tests on different samples of un-coated and Cr-coated (less optimized coating) Zircaloy-4 substrates the current Cr-coated sample (more optimized coating) has not shown any visual large cracking after the three stages, other than a small region near the end cap. The previous coated samples had a crack initiated near the end cap which moved upward, likely due to the different crystal orientation of the end cap in comparison with the tubular part. However, the sample bent during the test as some stress was applied to hold the sample on the alumina mounts, and the tube deformed due to Zircaloy high-temperature thermal creep. A picture of the sample during the air quenching was taken after each stage (Fig. 4). Colour on the tube varied along the tube, since only the bottom 10 cm of the sample was exposed to 1200 °C. A small crack was observed at the endcap region where the sample was bent. The sample in this region was very brittle and fragile.

Fig. 4: Cr-coated steam oxidized samples during air-quenching.

After oxidation, the sample was cut using a low speed saw with a diamond blade, mounted, polished, and observed under a JEOL JSM-6610LV scanning electron microscope (SEM) system equipped with an energy dispersive spectroscopy (EDS) device. It has to be mentioned that the region near the end cap was too fragile to survive cutting, so fractured pieces were mounted in epoxy and polished afterwards. Fig. 5 shows an SEM image of that region, where Zircaloy-4 substrate is on the left side of the image. The oxide thickness was significantly reduced by the protective Cr layer in comparison with previous results of uncoated Zircaloy-4 samples [13]. An oxide thickness of 249 microns was observed beneath the Cr layer, where the oxide thickness on an uncoated Zircaloy-4 was 429 microns.

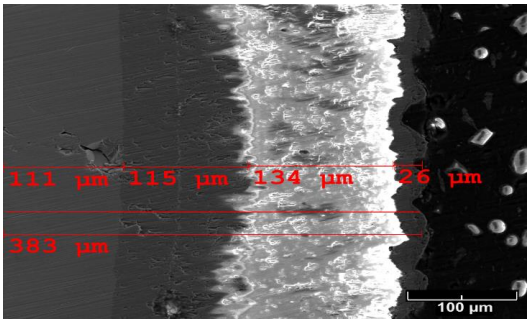

Fig. 5: SEM image of steam-oxidized Cr-coated tube near the end cap.

3.2 Surface Characterization

The static contact angle of Zircaloy-4 was 83° ± 3° whereas for the Cr coated Zircaloy-4 sample was 86° ± 4°. Here the "± value" represents the standard deviation of multiple measurements, and is represented in Fig. 6. as the error bars. Measurement of the contact angle was also performed for a 99.9% pure chrome rod and was 92° ± 4°. Thus, the tested wettability of the chrome coating on Zircaloy-4 was in the range intermediate to that of pure chrome and Zircaloy-4. The average surface roughness (R_a values) are shown in Table 1. All the tested samples had the same order of roughness and thus the impact of surface roughness in the present work can be assumed as negligible. The gamma samples were irradiated in the gamma cell for 96 hours and the contact angle measurement was taken after every 24 hours during irradiation. The contact angles of irradiated samples continuously decreased as shown in Fig. 6 . After 96 hours, the Cr samples which initially had a higher contact angle when compared to Zircaloy-4 reached a superhydrophillic state. The improved wettability under irradiation phenomenon for oxidized samples has been evident in the previous works [14] [15]. However, from the present experiments, it is clear that irradiation has a dominant role in increasing the wettability of non-oxidized samples as well.

Table 1: Surface Roughness of Tested samples.

Sample	Average Surface Roughness (R_a) (μm)
Zirc-4	0.32
Cr Coated	0.41
Pure Cr	15

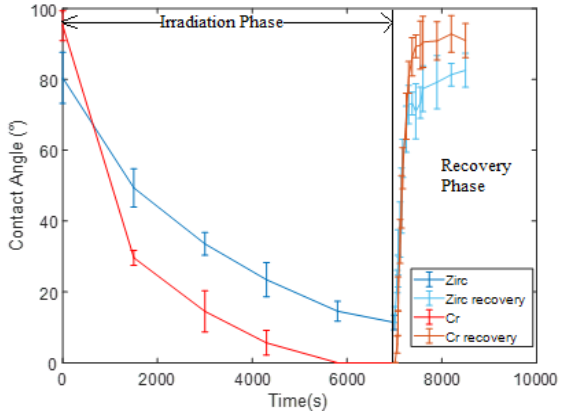

Fig. 6: Decrease in contact angle on samples exposed to gamma irradiation and increase (recovery) in contact angle of samples after gamma irradiation.

The trend in contact angle can also be observed in the capillary wicking test carried out on the samples. Table 2 shows that the capillary wicking in the Cr samples was enhanced considerably (nearly 4 times) immediately after gamma irradiation. Zircaloy-4 also saw an increase in capillary wicking but to a much smaller extent when compared to the chrome coated Zircaloy-4 sample. The primary mechanism behind improved wettability has been found to be the formation of oxides on the surface under gamma irradiation in air. While the hydrophobic

recovery is attributed to contamination of the surface by organic materials in air. For further detail, reference [16] and [17] can be referred.

Table 2: Capillary wicking

Sample	Wicking (mm^3/s) As Machined	Wicking (mm^3/s) Immediately After Gamma Irradiation
Zircaloy-4	4.5	5.4
Cr Coated	2.3	8.1

The irradiated samples were quenched in a saturated pool of water. Fig. 7 shows the centerline temperature history during the quenching of the non-irradiated and irradiated samples. During the vertical quenching of a rodlet, the heat transfer depends on the various boiling regimes. The initial dominant mechanism for heat transfer was film boiling, in which the cooling rate is slow and can be seen in Fig. 7 by the initial slope of the curve. The vapor trapped at the surface of the rod reduced the heat transfer from the heated rod to the coolant in the quench pool. However, after the Leidenfrost temperature was reached, i.e the temperature at which the slope changes in the graph shown in Fig. 7, there is a transition from film boiling to nucleate boiling. The nucleate boiling starts at the bottom of the rodlet and propagates upward.

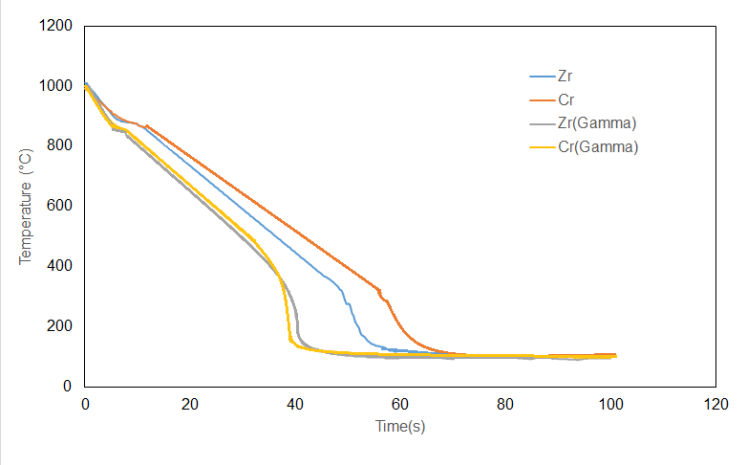

Fig. 7: Quench time history for non-irradiated samples, gamma irradiated samples

Fig. 7 shows that the quench curves of gamma-irradiated samples have shifted to the left indicating better quench cooling. It can be observed from Fig. 7 that the overall quenching time of gamma-irradiated chrome coated sample is slightly less than that of gamma-irradiated Zircaloy-4. The irradiated samples have a higher Leidenfrost temperature as well as quench front speed when compared to as received samples. Again one can intuitively understand the higher Leidenfrost temperature and quench front speed on irradiated samples are a result of increased wettability and capillary wicking as discussed previously. Fig. 7 demonstrate that irradiation speeds quenching and improves surface wettability and wicking of the Cr coated Zircaloy-4 sample to a larger degree than for the Zircaloy-4 sample. Thus, one can infer that the thermal-hydraulic performance of Cr-coating in a nuclear reactor environment is similar or superior to that of Zircaloy-4 due to presence of intense gamma rays.

3.3 Burst

The burst tests were carried out on Zircaloy-4 tubes with and without chromium coating. Their lengths range from 48 mm to 52 mm and the coating thickness is approximately 25 μm all around the tube. Scanning electron microscopy was used to explore the effect of burst on surfaces of individual samples. Fig. 8 and 9 illustrate the surface of chromium coating before and after the burst experiment. It can be observed that the coating surface after the burst experiment is less coherent but intact.

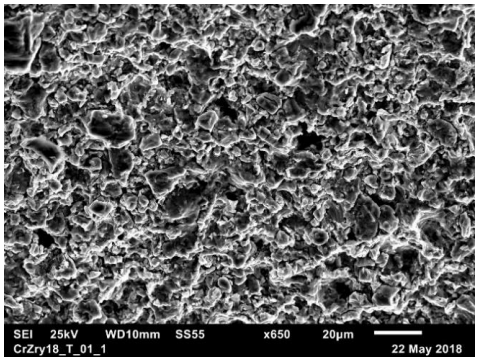

Fig. 8: Surface of Zircaloy tube with chromium coating before the burst experiment.

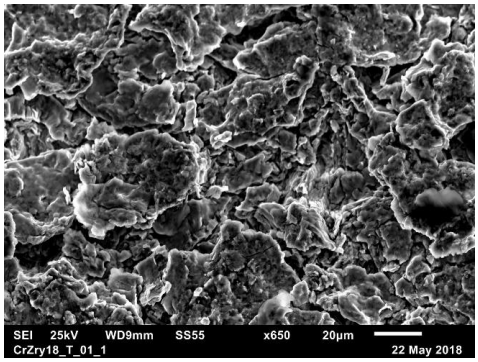

Fig. 9: Bulge surface of Zircaloy tube with chromium coating after the burst experiment.

The overall results are summarized in Table 3. The additional chromium coating did not result in any noticeable increase in burst pressure (+4%) and UTS pressure (+0.5%), respectively. The crack length was also on the same order, with the coating slightly longer.

Table 3: Average results for a total of 7 pure Zircaloy-4 samples, 3 Zircaloy-4 samples with Cr coating, and their standard deviations.

	OD (mm)	Thickness (mm)	UTS Pressure (MPa)	UTS (MPa)	Burst Pressure (MPa)	Crack length (mm)	Bulge diameter (mm)	Crack opening (mm)
Zircaloy-4	9.47	0.59	102.61	770.55	87.62	18.6	16.38	1.9
Standard deviation	0.01	0.02	0.80	22.44	3.17	0.95	0.42	0.20
Zircaloy-4 + Cr	9.52	0.59	103.12	779.54	91.15	20.3	16.39	2.4
Standard deviation	0.03	0.02	0.52	19.57	1.02	0.20	0.21	0.31

4 Conclusions

In this work, a more optimized Cold-spray chromium cladding was fabricated relative to the previous study. Since the rod and the endcaps were fully coated, when exposed to 1200 ^{o}C, the sample underwent large strains due to the unoxidized Zircaloy-4 high thermal creep strain.

This resulted in bending of the rod since Cr only forms a thin oxide layer during 90 min of exposure to 1200 °C steam relative to Zircaloy-4. This added ductility needs to be considered when assessing the safety performance of coated cladding. The expected in reactor thermal hydraulic performance of Cr coating should be similar to Zircaloy based on detailed surface characterization, film and nucleate boiling rates during the quench performance. The 25 um coating as expected, did not change the burst pressure nor the burst characteristics at room temperature and adhered to the sample. At the time of submission of this paper, unsuccessful attempts were made in the investigation of the coated cladding performance at > 1300 °C. That still remains an important area of future work.

Acknowledgements

The support for this work was provided by the US Department of Energy Integrated Research Project (IRP) Grant: DE-NE0008416.

5 References

[1] J. Carmack, F. Goldner, S. M. Bragg-Sitton, and L. L. Snead, "Overview of the US DOE accident tolerant fuel development program," in Proc. 2013 LWR Fuel Performance Meeting/TopFuel 2013, 2013, pp. 15-19.
[2] J. Bischoff et al., "Development of Cr-coated zirconium alloy cladding for enhanced accident tolerance," pp. 1165-1171, 2016.
[3] B. Maier et al., "Development of cold spray coatings for accident-tolerant fuel cladding in light water reactors," vol. 70, no. 2, pp. 198-202, 2018.
[4] H.-G. Kim, I.-H. Kim, Y.-I. Jung, D.-J. Park, J.-Y. Park, and Y.-H. J. J. o. N. M. Koo, "Adhesion property and high-temperature oxidation behavior of Cr-coated Zircaloy-4 cladding tube prepared by 3D laser coating," vol. 465, pp. 531-539, 2015.
[5] A. Kuprin et al., "Vacuum-arc chromium-based coatings for protection of zirconium alloys from the high-temperature oxidation in air," vol. 465, pp. 400-406, 2015.
[6] Y. Wang et al., "Behavior of plasma sprayed Cr coatings and FeCrAl coatings on Zr fuel cladding under loss-of-coolant accident conditions," vol. 344, pp. 141-148, 2018.
[7] M. Ševeček et al., "Development of Cr cold spray–coated fuel cladding with enhanced accident tolerance," Nuclear Engineering and Technology, vol. 50, no. 2, pp. 229-236, 2018.
[8] ASTM B614-16 Standard Practice for Descaling and Cleaning Zirconium and Zirconium Alloy Surfaces., 2016.
[9] P. Guenoun, "Design optimization of advanced PWR SiC/SiC fuel cladding for enhanced tolerance of loss of coolant conditions," Massachusetts Institute of Technology, 2016.
[10] G. W. Daines, "Evaluation of multilayer silicon carbide composite cladding under loss of coolant accident conditions," Massachusetts Institute of Technology, 2016.
[11] J. Cathcart et al., "Zirconium metal-water oxidation kinetics. IV. Reaction rate studies," Oak Ridge National Lab.1977.
[12] M. M. Rahman, E. Olceroglu, and M. McCarthy, "Role of wickability on the critical heat flux of structured superhydrophilic surfaces," Langmuir, vol. 30, no. 37, pp. 11225-11234, 2014.
[13] A. Gurgen, "Estimation of coping time in pressurized water reactors for near term accident tolerant fuel claddings," SM, Nuclear Science and Engineering, Massachusetts Institute of Technology, Cambridge MA USA, 2018.

[14] T. Takamasa, T. Hazuku, K. Mishima, K. Okamoto, and Y. Imai, "Surface wettability caused by radiation induced surface activation," Thermal Science and Engineering, vol. 12, no. 2, pp. 39-44, 2004.
[15] T. Takamasa, T. Hazuku, K. Okamoto, K. Mishima, and M. Furuya, "Radiation induced surface activation on Leidenfrost and quenching phenomena," Experimental Thermal and Fluid Science, vol. 29, no. 3, pp. 267-274, 2005.
[16] A. Seshadri, B. Phillips, K. Shirvan, and M. Transfer, "Towards understanding the effects of irradiation on quenching heat transfer," vol. 127, pp. 1087-1095, 2018.
[17] A. Seshadri, K. Shirvan, and Design, "Quenching heat transfer analysis of accident tolerant coated fuel cladding," vol. 338, pp. 5-15, 2018.